Primary and Secondary Processes in the Photodissociation of $CHBr_3$†

W. Sean McGivern,‡ Osman Sorkhabi,§ Arthur G. Suits,§ Agnes Derecskei-Kovacs,‡ and Simon W. North*,‡

Department of Chemistry, Texas A&M University, College Station, Texas 77842, and Chemical Sciences Division, Lawrence Berkeley Laboratory, and Chemistry Department, University of California, Berkeley, California 94720

Received: February 8, 2000; In Final Form: April 4, 2000

The photodissociation of $CHBr_3$ at 193 nm has been investigated using photofragment translational spectroscopy with VUV ionization detection. The only primary process observed was the loss of bromine atom. The translational energy distribution for this channel suggests a direct dissociation from an excited electronic state, and the anisotropy parameter, $\beta = 0.0$, is consistent with a transition dipole moment aligned perpendicular to the C_{3v} axis. The majority of nascent $CHBr_2$ fragments undergo secondary dissociation via two competing channels. The elimination of HBr and C−Br bond cleavage in $CHBr_2$ occur with comparable yields. We also provide ab initio calculations on the relevant photochemical species and RRKM estimates of the product branching ratios that are consistent with the experimental observations.

I. Introduction

The role of anthropogenic and natural sources of chlorine-containing molecules in stratospheric ozone depletion has been well established.[1] The influence of bromine and its chemistry on the atmosphere, however, has received considerably less attention. Bromine in the stratosphere depletes ozone via a chain reaction mechanism analogous to the well-known ClO_x cycle.

$$Br + O_3 \rightarrow BrO + O_2$$

$$BrO + O \rightarrow Br + O_2$$

Although the concentration of bromine in the stratosphere is much lower than that of chlorine, the reservoir species that temporarily confine reactive bromine are photochemically labile and, therefore, inefficient. As a result, bromine is far more destructive to stratospheric ozone than chlorine on an atom-for-atom basis.[2] Recent estimates by Garcia and Solomon report that each Br atom could be as much as 100 times more destructive, suggesting that bromine may be as important in stratospheric ozone depletion as chlorine.[3] In addition to catalytic bromine cycles, the coupling of the BrO and ClO cycles to produce free bromine and chlorine atoms via the reaction

$$BrO + ClO \rightarrow Br + Cl + O_2$$

can enhance the depletion of ozone by chlorofluorocarbons by up to 20% for even moderate mixing ratios of bromine in the stratosphere. Despite the significance of bromine-containing compounds, there is a severe lack of experimental data regarding the photodissociation of these molecules.

Bromoform is one of several volatile halocarbon compounds that contribute active bromine to the atmosphere. It is primarily of biogenic origin and is produced in the Arctic by both kelp and ice algae as a byproduct of photosynthetic processes.[4] Other natural sources include emissions from oceanic microalgae, which result in large concentrations of bromocarbons in the marine boundary layer.[5] Of the bromomethane derivatives, bromoform has been found to be the greatest contributor of bromine to the Arctic atmosphere,[6] with an atmospheric lifetime of approximately two weeks.[7] Despite its importance, relatively few studies of bromoform photochemistry have been performed. At wavelengths near 200 nm, there are several energetically accessible dissociation pathways, including both two-body and three-body processes.

$$CHBr_3 \rightarrow CHBr_2 + Br(^2P_J) \quad (J = {}^1/_2, {}^3/_2) \qquad (1)$$

$$\rightarrow CHBr + Br_2 \qquad (2)$$

$$\rightarrow CBr_3 + H \qquad (3)$$

$$\rightarrow CBr_2 + HBr \qquad (4)$$

$$\rightarrow CBr + HBr + Br \qquad (5)$$

$$\rightarrow CHBr + Br + Br \qquad (6)$$

Simons and Yarwood have studied the photodissociation of $CHBr_3$ using flash photolysis near 200 nm.[8] Spectral features corresponding to vibronic transitions associated with CBr were observed following photolysis. The authors asserted that the origins of CBr involved the primary loss of bromine atom followed by the spontaneous decomposition of the energized $CHBr_2$ radical. Power-dependence studies indicated that the CBr was the result of a single-photon process. Stern−Volmer experiments, performed by varying buffer gas pressures at several different excitation energies, and RRK calculations provided information on the threshold for CBr formation from $CHBr_2$. Sears and co-workers have subsequently used $CHBr_3$ phototolysis at 193 nm as a means of preparing CBr for infrared spectroscopic studies.[9] The authors were also able to obtain the CHBr radical from $CHBr_3$ at this wavelength and determined that the products also resulted from a single-photon process, suggesting an additional fate for the energized $CHBr_2$ radicals.[10,11]

† Part of the special issue "C. Bradley Moore Festschrift".

* Corresponding author. E-mail: north@mail.chem.tamu.edu.
‡ Texas A&M University.
§ University of California.

10.1021/jp0005017 CCC: $19.00 © 2000 American Chemical Society
Published on Web 05/13/2000

In the present paper, we examine the photodissociation of $CHBr_3$ at 193 nm. We find that the dissociation involves both primary and secondary fragmentation channels, resulting in bromine atom quantum yields greater than unity and in the release of HBr. The primary step in the dissociation is the rapid loss of atomic bromine, resulting in a $CHBr_2$ radical with sufficient internal energy to dissociate via the loss of Br and HBr with comparable yields. The use of VUV ionization, as opposed to electron impact, for product detection is ideally suited for studying complex multichannel dissociation processes, in which excessive dissociative ionization can significantly complicate the analysis. Analysis of such data, in addition to RRKM calculations using ab initio energies and geometries, permits a precise determination of the photofragment quantum yields and provides valuable thermodynamic information, including the barrier height for HBr elimination from $CHBr_2$.

II. Experimental Section

The fixed-detector/rotating-source molecular beam apparatus has been described in detail previously.[12] A continuous molecular beam of <1% bromoform seeded in helium was collimated with conical skimmers and intersected at 90° with the output of a Lambda Physik LPX-200 excimer laser operating on the ArF transition (193 nm). There was no change in the shape of any of the TOF spectra over a laser fluence range of 60−500 mJ/cm^2, providing strong evidence that all of the observed signals are the result of single-photon absorption. Neutral photodissociation products traveled 15.1 cm, to a region where they were ionized by tunable VUV undulator radiation, mass selected, and counted as a function of time. The characteristics of the VUV undulator radiation used for product photoionization have also been previously described.[13] The nozzle was heated to 100 °C to minimize clustering in the beam, and no evidence for clusters was observed. A pile-of-plates polarizer, consisting of eight quartz plates at Brewster's angle, was used to polarize the excimer beam, resulting in >85% linear polarization. Rotation of the linear polarized beam was achieved using a half-wave plate (Karl Lambrecht).

Bromoform 99% was obtained from Aldrich Chemical Co. and used without further purification.

III. Results and Analysis

Center-of-mass translational energy, $P(E_T)$, distributions were obtained from the time-of-flight (TOF) spectra using the forward convolution technique.[14] For all of the TOF spectra presented, the circles represent the data, and the lines represent the forward convolution fits.

TOF spectra were obtained for several masses: $CHBr^+$ (*m*/*z* 92), Br^+ (*m*/*z* 79 and 81), HBr^+ (*m*/*z* 80 and 82), and CBr^+ (*m*/*z* 91). No signal was observed for $CHBr_2^+$ (*m*/*z* 173) at VUV ionization energies from 15 to 8 eV. Although the ionization energy for $CHBr_2$ is 8.13 eV,[15] it is formed with an average internal energy (vide infra) that exceeds the threshold for $CHBr^+$ upon ionization above threshold.[16] As a result, this species contributes only to the *m*/*z* 92 ($CHBr^+$) TOF spectra. The ionization energy dependence of both the Br^+ and the HBr^+ signals showed no change in shape as the energy was varied from 15 to 12 eV, indicating that there is no contribution from dissociative ionization in these TOF spectra. No CBr_2^+ was detected (ionization energy of 10.1 eV), and no evidence of this fragment at lower masses was observed.

A. Primary Dissociation and Product Identification. TOF spectra for *m*/*z* 92 ($CHBr^+$) at laboratory angles of 10°, 15°, and 20° are shown in Figure 1. There are two contributions to the CHBr spectra. The first contribution, indicated by the solid line, results from the dissociative ionization of $CHBr_2$ fragments. The second contribution (dashed line) is from CHBr fragments that arise from the spontaneous dissociation of $CHBr_2$. Figure 2 shows the ionization dependence of the CHBr TOF spectra, which confirms the identity of the contributions. As the VUV energy is decreased to 11 eV, the contribution attributed to the $CHBr_2$ daughter fragments shows a significant decrease relative to that of the CHBr fragments. The ionization energy of CHBr is 8.94 eV,[17] and signals associated with this fragment persist near threshold, although the overall signal is greatly reduced. Figure 3 shows the Br^+ (*m*/*z* 79) TOF spectra at laboratory angles of 15° and 30° and a photoionization energy of 15 eV. There are also two contributions to the *m*/*z* 79 spectra: a fast contribution near the leading edge of the profile (solid line) and a contribution at longer times (dashed line). The fast component can be attributed to primary loss of Br from $CHBr_3$ and has been fit using the $P(E_T)$ distribution shown in the top panel of Figure 4. The $P(E_T)$ distribution is nearly Gaussian in shape, with a maximum at 13 kcal/mol and a fwhm of 8 kcal/mol. Indicated on the top axis is the $CHBr_2$ internal energy corresponding to the total translational energy, assuming that the bromine atom is formed in its ground spin−orbit state, $Br(^2P_{3/2})$. Only the fastest Br signal can be momentum-matched to the features assigned to $CHBr_2$ fragments in Figure 1. Shown in the bottom panel of the figure is the $P(E_T)$ distribution used to fit the primary $CHBr_2$ dissociation, which corresponds to a

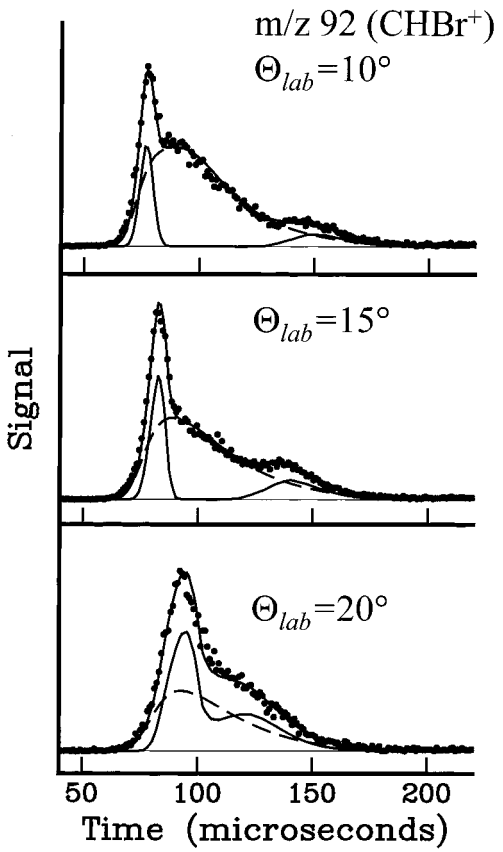

Figure 1. Unpolarized TOF spectra for *m*/*z* 92 ($CHBr^+$) photoproducts at scattering angles of 10°, 15°, and 20° and a photoionization energy of 15.0 eV. The circles are the experimental data, and the solid lines are the forward convolution fits using the $P(E_T)$ distributions in Figure 4.

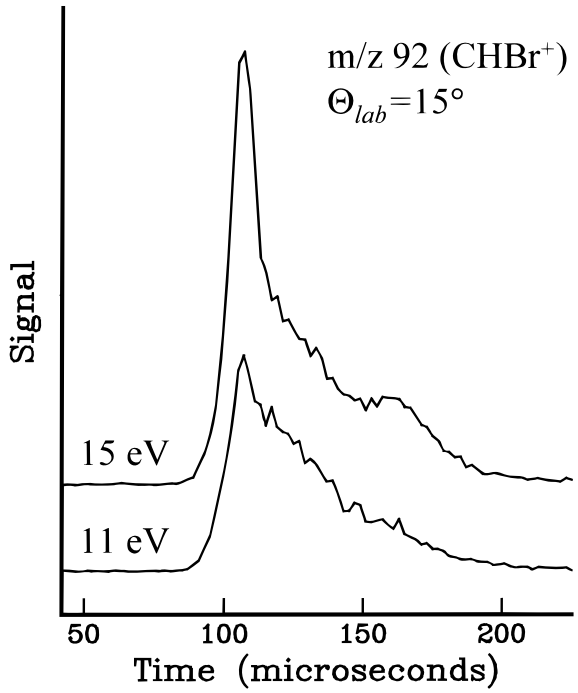

Figure 2. Experimental TOF spectra for *m*/*z* 92 ($CHBr^+$) at 15° and photoionization energies of 15.0 eV (top trace) and 8 eV (bottom trace).

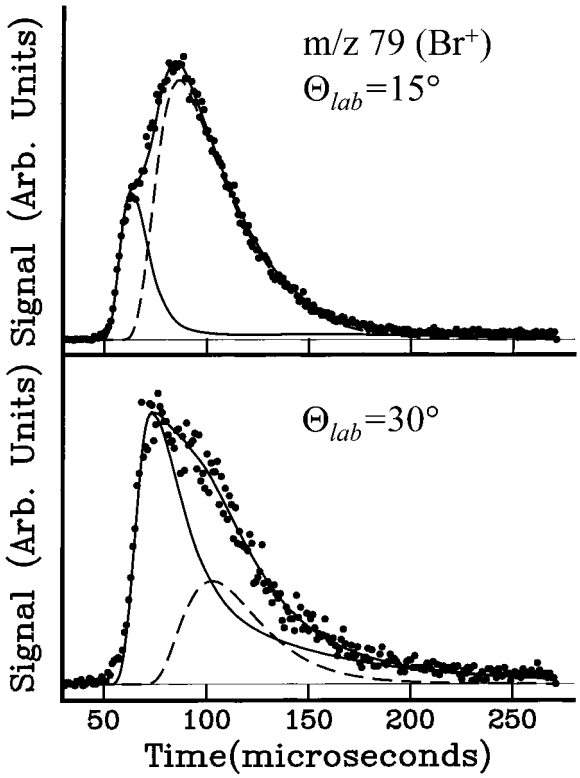

Figure 3. Unpolarized TOF spectra for *m*/*z* 79 (Br^+) at scattering angles of 15° and 30° and a photoionization energy of 15.0 eV. The circles are the experimental data, the solid line is the forward convolution fit using the $P(E_T)$ distribution shown in top panel of Figure 4, and the dashed line is the contribution from secondary Br loss from the $CHBr_2$ radical.

threshold for secondary dissociation near 68 kcal/mol.[18] The fits to the *m*/*z* 92 TOF spectra are extremely sensitive to changes in the leading edge of the $CHBr_2$ $P(E_T)$ distribution, providing a good estimate of the threshold energy. Although HBr fragments are detected, they cannot be attributed to a primary dissociation channel. Therefore, we find that the only observed

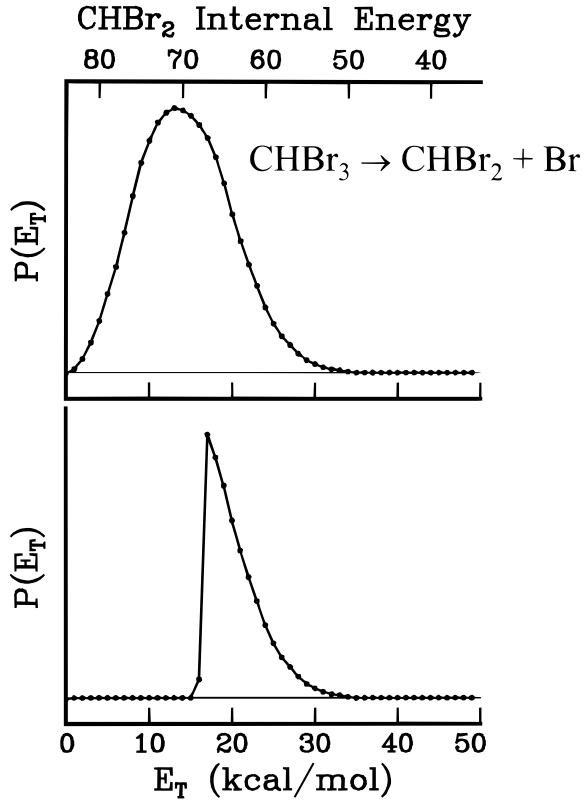

Figure 4. The upper panel shows the primary $P(E_T)$ distribution used to fit the fastest Br contribution in the TOF spectra in Figure 3. The internal energy of the $CHBr_2$ radical, formed in coincidence with ground-state bromine, is indicated on the top axis. The lower panel shows the primary $P(E_T)$ distribution used to fit the $CHBr_2$ contribution to the *m*/*z* 92 TOF spectra in Figure 1.

primary channel is the loss of bromine atom, and the remaining products are the result of secondary processes.

Photofragment angular distributions were recorded as a function of laser polarization using the leading edges of the Br^+ and $CHBr^+$ signals at a laboratory angle of 10°. The laboratory angular distributions, $I(\theta)$, are given by

$$I(\theta) = \frac{1}{4\pi}[1 + \beta P_2(\cos\theta)]$$

where β is the anisotropy parameter and $P_2(x)$ is the second Legendre polynomial. For prompt dissociation in the axial recoil limit, the anisotropy parameter is given by $\beta = 2P_2(\cos\chi)$, where χ is the angle between the recoil velocity vector and the transition dipole moment. No polarization dependence was observed for either mass, corresponding to an anisotropy parameter of $\beta = 0.0 \pm 0.1$.

B. Secondary Dissociation of the $CHBr_2$ Radical. The lack of momentum matching between the Br and $CHBr_2$ fragments is strong evidence for secondary dissociation. Only the Br loss channel (eq 6) and the HBr elimination channel (eq 5) are energetically accessible at 193 nm, and we see evidence for both channels in the TOF spectra. The forward convolution fitting of secondary dissociation processes has been discussed in detail previously.[19,20] A primary $P(E_T)$ distribution is first chosen to represent the translational energy of the primary fragments that undergo secondary decomposition. In principle, this can be determined by subtracting the $P(E_T)$ distribution derived from fitting the $CHBr_2$ fragment from the $P(E_T)$ distribution for the Br fragment. There are two secondary channels, however, each with a different energetic threshold.

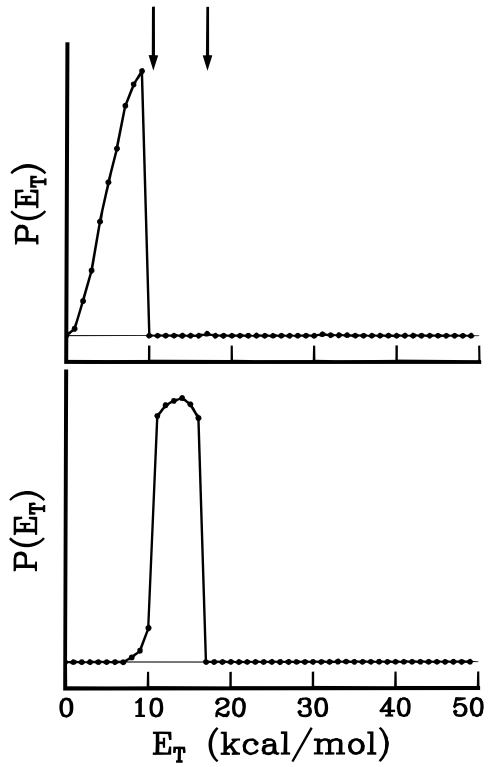

Figure 5. The upper panel shows the primary $P(E_T)$ distribution used to model the secondary Br loss from $CHBr_2$. The lower panel shows the primary $P(E_T)$ distribution used to model the HBr elimination from $CHBr_2$. The thresholds for secondary Br and HBr loss are indicated by the arrows in the upper panel.

As a consequence, the leading edge of the distribution in the lower panel of Figure 4 corresponds only to the lowest threshold process. We have relied on ab initio and RRKM calculations (vide infra) to provide additional information for assigning these thresholds. We find that the threshold for HBr loss is lower in energy (68.0 kcal/mol) than that for Br elimination (73.6 kcal/mol), and therefore, the abrupt truncation point in the $CHBr_2$ $P(E_T)$ distribution corresponds to the onset of HBr loss. On the basis of RRKM calculations, discussed in detail below, we find that, once the Br loss channel is energetically accessible, it becomes the dominant dissociation pathway for $CHBr_2$. Therefore, primary $CHBr_2$ fragments with internal energies greater than the HBr loss threshold but less than the Br loss threshold contribute to channel 5, while the $CHBr_2$ fragments with internal energy greater than the Br loss threshold contribute only to channel 6. The resulting primary $P(E_T)$ distributions for each secondary channel are shown in Figure 5 and provide very good fits to the data. It should be noted that initial attempts to iteratively fit the data without the ab initio constraints resulted in quantitatively similar distributions, providing additional support for the locations of the secondary thresholds.

The secondary dissociation lifetimes for both channels were assumed to exceed the rotational period, resulting in a forward−backward symmetric secondary angular distribution.[21,22] Fits to the TOF spectra for each secondary channel were obtained by iteratively adjusting the secondary angular distribution (maintaining forward−backward symmetry) and the secondary $P(E_T)$ distribution. Fragments associated with the Br loss channel appear as the central feature in the $CHBr^+$ spectra and as the slow feature in the Br^+ spectra (Figures 2 and 3, respectively). The best-fit secondary $P(E_T)$ distribution for this channel is shown in the top panel of Figure 6. Fragments arising from the HBr elimination channel represent the sole contributions to the

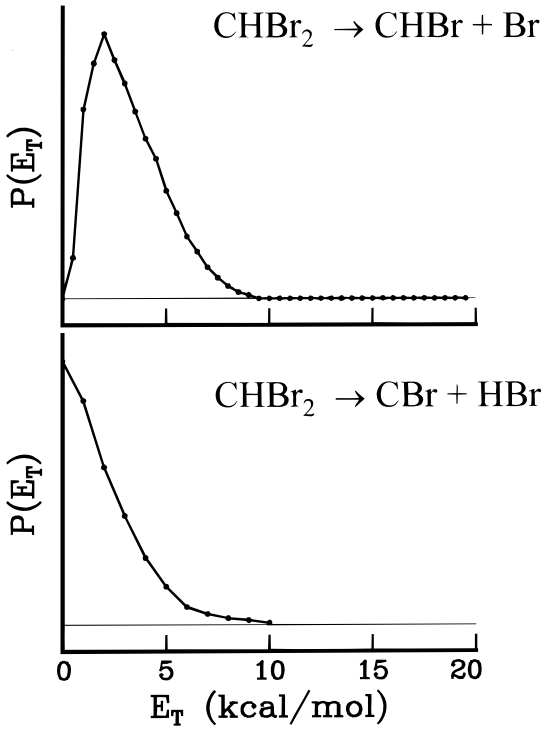

Figure 6. The upper panel shows the secondary $P(E_T)$ distribution corresponding to Br loss from the $CHBr_2$ radical. The lower panel shows the secondary $P(E_T)$ distribution for HBr elimination from $CHBr_2$.

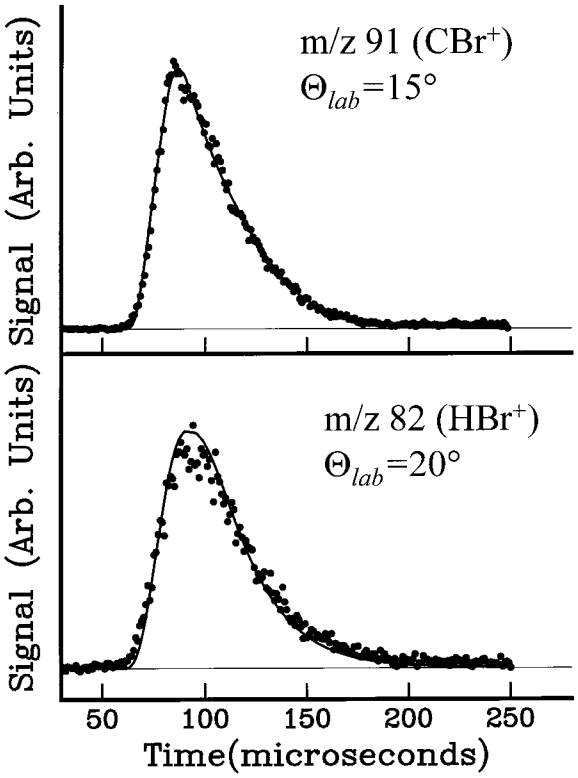

Figure 7. Experimental TOF spectra for *m/z* 91 (CBr^+) at 15° (upper panel) and for *m/z* 82 (HBr^+) at 20°(lower panel) for a photoionization energy of 15.0 eV. The circles are the experimental data, and the solid lines are the forward convolution fits to the data using the primary $P(E_T)$ distribution in the lower panel of Figure 5 and the secondary $P(E_T)$ distribution in the lower panel of Figure 6.

HBr^+ and CBr^+ TOF spectra shown in Figure 7. The secondary $P(E_T)$ for the HBr loss channel is shown in the bottom panel of Figure 6. Both distributions peak at low translational energies,

suggesting almost no barrier to recombination. On average, there is little energy (<19 kcal/mol) available for the fragments of secondary dissociation. The sensitivity of the fits to the secondary $P(E_T)$ distributions is modest and depends on the choice of each corresponding primary $P(E_T)$. However, the qualitative result that both are peaked near zero is robust.

IV. Discussion

A. Primary Dissociation Mechanism. The measured isotropic spatial distribution of the photofragments could be the result of several factors. If the dissociation is not prompt on the time scale of parent rotation, the correlation between the direction of the electric dipole moment and the relative velocity will be diminished by parent rotation. On the basis of previous work on halogenated methane derivatives[23] and the observed translational energy distribution, however, we believe that the primary dissociation is direct, involving excitation to a repulsive state. The impulsive model, which provides an adequate description of direct dissociation, predicts an average translational energy of 16 kcal/mol, in reasonable agreement with the measured value. A fast dissociation can also produce an isotropic velocity distribution if the angle between the recoil direction and the transition dipole moment, χ, is 54.7°. In C_{3v} symmetry, an $A_1 \leftarrow A_1$ transition requires that the transition dipole moment lie along the 3-fold axis, which, on the basis of an ab initio geometry optimization of $CHBr_3$, gives a value of $\chi = 72.7°$, resulting in an anisotropy parameter of $\beta = -0.73$. The dipole moment for an $E \leftarrow A_1$ transition is perpendicular to this axis, which yields $\beta = -0.05$ after averaging over the azimuthal orientation of the bromine atoms. This result is consistent with our observations.

Although there is no direct experimental evidence, we do not expect that spin−orbit excited bromine, $Br(^2P_{1/2})$, is formed in significant yield. The truncation of the primary $P(E_T)$ distribution required to fit the $CHBr_2$ contribution shown in Figure 1 is very abrupt. The formation of substantial excited-state bromine would result in stable $CHBr_2$ with translational energies approaching zero, which is not observed. In addition, the quantum yields for primary and secondary Br are more consistent with the absence of excited Br. We are unable, however, to rule out a minor contribution of excited-state bromine. State-selected experiments could provide a definitive determination of the spin−orbit branching in the dissociation.

B. Ab initio and RRKM Calculations on the Dissociation of $CHBr_2$. To understand more about the photodissociation of $CHBr_3$ and, in particular, the competition between secondary dissociation channels, we have performed ab initio and RRKM calculations. All ab initio calculations were performed using Gaussian 94[24] on an Origin 2000 supercomputer and an SGI Power Challenge workstation. Geometries and frequencies for the ground-state species were calculated at the MP2/6-311+G* level, and vibrational frequencies were left unscaled for the zero-point corrections and RRKM calculations. The transition state for the HBr loss channel was optimized at the MP2/6-31+G* level, and single-point energies were calculated at the MP2/cc-pVtz level. Relevant geometries for the secondary dissociation products and the transition state are shown in Figure 9. Recently, a methodology has been developed to correct carbon−halogen bond energies for basis-set effects beyond the triple-ζ level and correlation effects beyond the MP2 approximation by applying corrections to the MP2/cc-pVtz energies.[25] Using this methodology, we have calculated final zero-point corrected C−Br bond energies of 63.8 and 73.6 kcal/mol for $CHBr_3$ and $CHBr_2$, respectively. The former value was calculated previously[25] and

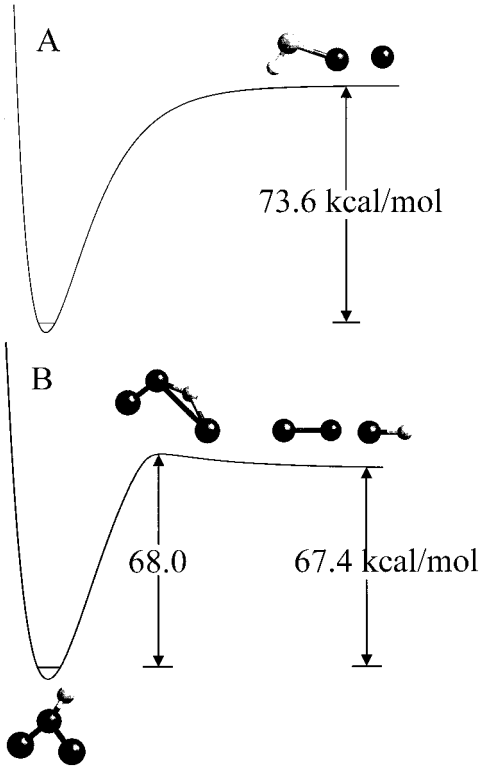

Figure 8. Schematic energy diagrams for the secondary dissociation of the $CHBr_2$ radical. The energies are the result of ab initio calculations, as described in the text.

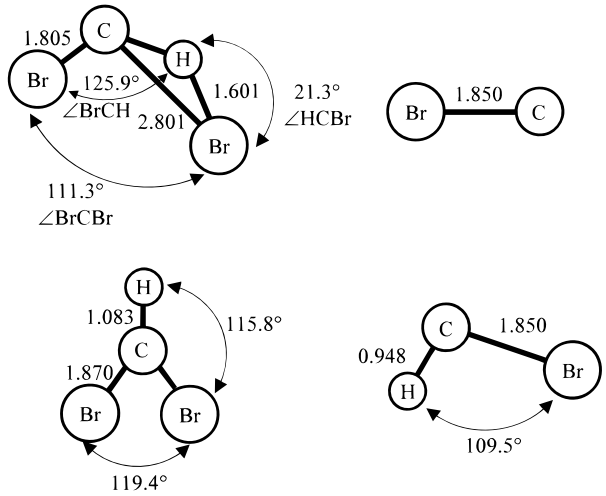

Figure 9. Optimized geometries of $CHBr_2$, CHBr, CBr, and the transition state for the HBr loss channel. Lengths are in angstroms, and angles are in degrees. The $CHBr_2$ radical shows a slight nonplanarity, with an angle of 33.0° between the two HCBr planes.

is in good agreement with previous theoretical[26] (62.7 ± 0.9 kcal/mol) and experimental[27] (66 ± 4 kcal/mol) results. The HBr loss channel is endothermic with a reaction energy of 67.4 kcal/mol, which is very close to previous reports,[28] and a barrier height of 68.0 kcal/mol. Calculated energies are shown schematically in Figure 8. The very small exit barrier from the three-center elimination of HBr is consistent with previous reports of three-center hydrogen halide elimination. Riehl and Morokuma have examined the three-center elimination of HCl from vinyl chloride.[29] The calculated transition state is qualitatively similar to the HBr transition state of the present study, with an elongated carbon−halogen bond length and a modestly lengthened C−H bond (Figure 9). The exit barrier for HCl loss was

TABLE 1: RRKM and Var-RRKM Microcanonical Rates for the Dissociation of $CHBr_2$

E* (kcal/mol)	E_T[a] (kcal/mol)	$k(CHBr_2 \rightarrow CBr + HBr)$ (s^{-1})	$k(CHBr_2 \rightarrow CHBr + Br)$ (s^{-1})
84	0.2	6.95×10^{11}	1.94×10^{13}
83	1.2	5.70×10^{11}	1.56×10^{13}
81	3.2	3.69×10^{11}	1.02×10^{13}
79	5.2	2.24×10^{11}	6.01×10^{12}
77	7.2	1.25×10^{11}	3.01×10^{12}
75	9.2	6.18×10^{10}	1.26×10^{12}
73	11.2	2.59×10^{10}	–
71	13.2	8.25×10^{9}	–
69	15.2	1.47×10^{9}	–

[a] Total translational energy for the $CHBr_2$ and Br fragments following 193 nm photodissociation of $CHBr_3$.

calculated to be only 2.6 kcal/mol above the asymptotic products. In the present study, the HBr loss channel from $CHBr_2$ is found to be only 0.6 kcal/mol higher than the asymptotic product energy. The smaller barrier found for $CHBr_2$ is not surprising given that the bromine atom can interact with the hydrogen atom more readily in the present system because of its larger size and relative proximity to the reacting hydrogen in a tetrahedral geometry.

Microcanonical unimolecular rates, $k(E, J)$, have been evaluated using RRKM and variational RRKM calculations[30] to describe the HBr and Br loss channels, respectively. For consistency, all frequencies and energies used in the RRKM calculations, including those for reactant and product species, were obtained from ab initio theory. A direct-count algorithm was used to determine the sum of states using the harmonic oscillator approximation for both sets of calculations. The rate of HBr loss was calculated using the optimized ab initio transition state geometries and frequencies.

Calculations of the unimolecular rates for the Br elimination channel were performed using variational RRKM theory,[30] minimizing the sum of states along the reaction coordinate.

$$\frac{dN^{\ddagger}(E, J, R^{\ddagger})}{dR} = 0$$

The frequencies of the transitional modes were assumed to change smoothly according to

$$\upsilon_i(R) = \upsilon_i(R_e) \exp(-aR)$$

where R_e is the equilibrium C−Br bond length and a is a constant taken to be 1.2.[31,32] The sum of a Morse function and a centrifugal barrier was used to model the potential along the C−Br stretching coordinate. The centrifugal barrier was derived using the average rotational energy of the $CHBr_2$ fragment corresponding to $J = 111$, derived from the soft-fragment impulsive model[33] following primary loss of bromine. Moments of inertia at each fixed geometry were obtained by changing only the C−Br bond length. One rocking mode and one wagging mode were treated as transitional modes. The remaining modes were assumed to be well-represented by the product frequencies.

RRKM and variational RRKM calculations were performed at a series of energies above the respective threshold energies for the HBr and Br channels corresponding to the measured $CHBr_2$ internal energy distribution. Table 1 summarizes the results as a function of the internal energy of the $CHBr_2$ fragment after the initial Br loss from $CHBr_3$. Rates for Br loss increase from 1×10^{12} s^{-1} to 2×10^{13} s^{-1} for energies above the threshold up to 10 kcal/mol. Rates for HBr elimination range from 1.5×10^{9} s^{-1} near the threshold to 7×10^{11} s^{-1} at the maximum energies available. Clearly, for $CHBr_2$ internal energies above the threshold for Br loss, the rate of Br loss exceeds the rate for HBr elimination by more than an order of magnitude. As a result, $CHBr_2$ fragments with internal energies above 73.6 kcal/mol will predominately form CHBr + Br. The collision frequency at ambient tropospheric conditions at 300 K is on the order of 10^9 s^{-1}, suggesting that $CHBr_2$ radicals with internal energies above the Br threshold will not be collisionally stabilized. However, $CHBr_2$ fragments with internal energies near the HBr elimination threshold may be quenched prior to reaction. This is consistent with the work of Simons and Yarwood,[8] who observed pressure-dependent quantum yields for the CBr products in $CHBr_3$ dissociation near 200 nm. Given that the peak of the $P(E_T)$ distribution for $CHBr_2$ is near this threshold, a significant fraction of $CHBr_2$ fragments may be expected to be stabilized in the atmosphere, in contrast to the collisionless conditions present in a molecular beam experiment.

C. Product Branching Ratios. We can estimate the branching ratio for the secondary dissociation channels and obtain Br and HBr quantum yields using the primary $P(E_T)$ distributions used to fit the TOF spectra. Assuming that the quantum yield for the primary bromine atoms is unity, the quantum yields for secondary Br and HBr can be determined by integrating the normalized $P(E_T)$ distribution in the top panel of Figure 4 over the limits illustrated in Figure 5 for each secondary channel. This analysis gives quantum yields for the secondary Br and HBr channels of 0.3 and 0.4, respectively. Therefore, the total yield for bromine atoms is 1.3 using this procedure. A quantum yield for Br atoms based on the relative contributions of primary and secondary channels to the Br TOF spectra is consistent with this value, although this value is slightly higher than that obtained from the $P(E_T)$ distributions. The observation of bound $CHBr_2$ in the m/z 92 ($CHBr^+$) TOF spectra and the location of the lower threshold to secondary dissociation provide an upper limit of 1.7 to the Br quantum yield. Because Br loss via a barrierless dissociation from $CHBr_2$ dominates HBr elimination above threshold and significant secondary HBr is observed, it is unlikely that the Br quantum yield is close to this upper bound. We, therefore, assign a quantum yield of 1.5 ± 0.2, which reflects the upper and lower bounds of the analysis. Accordingly, we assign a final HBr quantum yield of 0.2 ± 0.2.

On the basis of our calculated thresholds, we can also comment on the wavelength dependence of the Br quantum yield. At wavelengths longer than 209 nm, there is insufficient energy for the formation of secondary Br, and the Br quantum yield should be unity. Above 218 nm, there is insufficient energy for the secondary dissociation of $CHBr_2$ toward HBr elimination, and only primary C−Br bond cleavage will occur. Of course, the precise quantum yields of Br and HBr at wavelengths shorter than these limits will depend intimately on the partitioning of the available energy in the primary dissociation step and will be more difficult to predict a priori. We note that Br loss from $CHBr_2$ should become increasingly dominant over HBr loss as the internal energy of the $CHBr_2$ radicals increases.

IV. Conclusions

The photodissociation of $CHBr_3$ has been investigated at 193 nm using photofragment translational spectroscopy with VUV ionization for product detection. We have identified and characterized both primary and secondary dissociation channels in the dissociation. The primary dissociation involves prompt C−Br bond fission. A fraction of the $CHBr_2$ radicals formed in the primary step contain sufficient energy to undergo spontaneous secondary dissociation via the elimination of both HBr and

Br to comparable extents. Ab initio calculations have provided important thermochemical information about the fragmentation of $CHBr_2$, including the transition state associated with HBr elimination. RRKM calculations have shown that significant secondary HBr may be formed in addition to secondary bromine fragments; however, under ambient tropospheric conditions, $CHBr_2$ fragments with internal energies below the Br-loss threshold may be collisionally stabilized prior to reaction.

Acknowledgment. Work by S.W.N. and W.S.M. was partially supported by a Research Enhancement from Texas A&M University. The work by A.G.S. and O.S. was supported by the Director, Office of Energy Research, Office of Basic Energy Science, Chemical Sciences Division of the U. S. Department of Energy under Contract DE-AC03-76SF00098. The experiments were conducted at the Advanced Light Source, Lawrence Berkeley National Laboratory, which is supported by the same source. Hardware and software support for the ab initio calculations was provided by the Texas A&M University Supercomputing Facility and Texas A&M University Laboratory for Molecular Simulations under National Science Foundation Grant CHE-9528196.

References and Notes

(1) Molina, M. J.; Rowland, F. S. *Nature* **1974**, *248*, 810.
(2) Solomon, S.; Mills, M.; Heidt, L. E.; Pollock, W. H.; Tuck, A. F. *J. Geophys. Res.* **1992**, *97*, 25.
(3) Garcia, R. R.; Solomon, S. *J. Geophys. Res*. **1994**, *99*, 12937.
(4) Cota, G. F.; Sturges, W. J. *Mar. Chem.* **1997**, *6*, 181.
(5) Class, T.; Kohnle, R.; Ballschmiter, K. *Chemosphere* **1986**, *15*, 429.
(6) Itoh, N.; Shinya, M. *Mar. Chem.* **1994**, *45*, 95.
(7) Barrie, L. A.; Bottenheim, J. W.; Schnell, R. C.; Crutzen, P. J.; Rasmussen, R. A. *Science* **1988**, *334*, 138.
(8) Simons, J. P.; Yarwood, A. J. *Trans. Faraday Soc.* **1961**, *57*, 2167.
(9) Marr, A. J.; Sears, T. J.; Davies, P. B. *J. Mol. Spectrosc.* **1997**, *184*, 413.
(10) Chang, B.-C.; Sears, T. J. *J. Chem. Phys.* **1996**, *105*, 2135.
(11) Marr, A. J.; North, S. W.; Sears, T. J.; Ruslen, L.; Field, R. W. *J. Mol. Spectrosc.* **1998**, *188*, 68.
(12) Yang, X.; Blank, D. A.; Lin, J.; Heimann, P. A.; Wodtke, A. M.; Suits, A.; Lee, Y. T. *Rev. Sci. Instrum.* **1997**, *68*, 3317.
(13) Koike, M.; Heimann, P. A.; Kung, A. H.; Namioka, T.; DiGennaro, R.; Gee, B.; Yu, N. *Nucl. Instrum. Methods Phys. Res.* **1994**, *347*, 282. Heimann, P. A.; Koike, M.; Hsu, C. W.; Evans, M.; Ng, C. Y.; Blank, D.; Yang, X. M.; Flaim, C.; Suits, A. G.; Lee, Y. T. *Proc. SPIE−Int. Soc. Opt. Eng.* **1996**, 2865.
(14) Zhao, X. Ph.D. Thesis, University of California, Berkeley, CA, 1989.
(15) Andrews, L.; Dyke, J. M.; Jonathan, N.; Keddar, N.; Morris, A. *J. Phys. Chem.* **1984**, *88*, 1950.
(16) The $CHBr_2^+$ is observed as a daughter fragment of $CHBr_3$ in on-axis TOF measurements to determine the velocity distribution of the molecular beam.
(17) Li, Z.; Francisco, J. S. *J. Chem. Phys.* **1998**, *109*, 134.
(18) For a discussion on obtaining thresholds for secondary processes using this approach, see: North, S. W.; Blank, D. A.; Lee, Y. T. *Chem. Phys. Lett.* **1994**, *224*, 38. Blank, D. A.; North, S. W.; Stranges, D.; Suits, A. G.; Lee, Y. T. *J. Chem. Phys.* **1997**, *106*, 539.
(19) Wodtke, A. M. Ph.D. Thesis, University of California, Berkeley, CA, 1986. Zhao, X. Ph.D. Thesis, University of California, Berkeley, CA, 1989.
(20) Zhao, X.; Nathanson, G. M.; Lee, Y. T. *Acta Phys.−Chim. Sin.* **1992**, *8*, 70.
(21) North, S. W.; Blank, D. A.; Lee, Y. T. *Chem. Phys. Lett.* **1994**, *224*, 38. Kroger, P. M.; Riley, S. J. *J. Chem. Phys.* **1977**, *67*, 4483.
(22) Hinsta, E. J.; Zhao, X.; Lee, Y. T. *J. Chem. Phys.* **1990**, *92*, 2280.
(23) Sparks, R. K.; Shobatake, K.; Carlson, L.R.; Lee, Y. T. *J. Chem. Phys.* **1981**, *75*, 3838. Gougousi, T.; Samartzis, P. C.; Kitsopolous, T. N. *J. Chem. Phys*. **1998**, *108*, 5742. McGivern, W. S.; Li, R.; Zou, P.; North, S. W. *J. Chem. Phys.* **1999**, *111*, 5771.
(24) Frisch, M. J.; Trucks, G. W.; Schlegel, H. B.; Gill, P. M. W.; Johnson, B. G.; Robb, M. A.; Cheeseman, J. R.; Keith, T.; Petersson, G. A.; Montgomery, J. A.; Raghavachari, K.; Al-Laham, M. A.; Zakrzewski, V. G.; Ortiz, J. V.; Foresman, J. B.; Cioslowski, J.; Stefanov, B. B.; Nanayakkara, A.; Challacombe, M.; Peng, C. Y.; Ayala, P. Y.; Chen, W.; Wong, M. W.; Andres, J. L.; Replogle, E. S.; Gomperts, R.; Martin, R. L.; Fox, D. J.; Binkley, J. S.; Defrees, D. J.; Baker, J.; Stewart, J. P.; Head-Gordon, M.; Gonzalez, C.; Pople, J. A. *Gaussian 94*, revision D.4; Gaussian, Inc.: Pittsburgh, PA, 1995.
(25) McGivern, W. S.; Derecskei-Kovacs, A.; North, S. W.; Francisco, J. F. *J. Phys. Chem. A* **2000**, *104*, 436.
(26) Paddison, S. J.; Tschuikow-Roux, E. *J. Phys. Chem*. **1998**, *102*, 6191.
(27) Miller, W. J.; Palmer, H. B. *J. Chem. Phys.* **1964**, *40*, 3701.
(28) The enthalpy of reaction for the reaction $CHBr_2 \rightarrow CBr + HBr$ can be determined to be 65.2 kcal/mol on the basis of a recent estimate for the heat of formation for $CHBr_2$ of 48.1 kcal/mol in ref 26.
(29) Riehl, J.-F.; Morokuma, K. *J. Chem. Phys.* **1994**, *100*, 8976.
(30) Holbrook, K. A.; Pilling, M. J.; Robertson, S. H. *Unimolecular Reactions*, 2nd ed.; Wiley-Interscience: New York, 1996. Forst, W. *Theory of Unimolecular Reactions*; Academic Press: New York, 1973.
(31) Hase, W. L. *Chem. Phys. Lett.* **1987**, *139*, 389.
(32) Sudbo, A. S.; Schultz, P. A.; Grant, E. R.; Shen, Y. R.; Lee, Y. T. *J. Chem. Phys.* **1979**, *70*, 921.
(33) Busch, G. E.; Wilson, K. R. *J. Chem. Phys.* **1972**, *56*, 3639.